
Neural Stethoscopes: Unifying Analytic, Auxiliary and Adversarial Network Probing

Fabian B. Fuchs Oliver Groth Adam R. Kosoriek Alex Bewley
Markus Wulfmeier Andrea Vedaldi Ingmar Posner

Department of Engineering Science
University of Oxford
{fabian,ogroth,adamk,bewley,markus,vedaldi,ingmar}@robots.ox.ac.uk

Abstract

Model interpretability and systematic, targeted model adaptation present central tenets in machine learning for addressing limited or biased datasets. In this paper, we introduce *neural stethoscopes* as a framework for quantifying the degree of importance of specific factors of influence in deep networks as well as for actively promoting and suppressing information as appropriate. In doing so we unify concepts from multitask learning as well as training with auxiliary and adversarial losses. We showcase the efficacy of neural stethoscopes in an intuitive physics domain. Specifically, we investigate the challenge of visually predicting stability of block towers and demonstrate that the network uses visual cues which makes it susceptible to biases in the dataset. Through the use of stethoscopes we interrogate the accessibility of specific information throughout the network stack and show that we are able to actively de-bias network predictions as well as enhance performance via suitable auxiliary and adversarial stethoscope losses.

1 Introduction

The advent of modern deep learning methods has exponentiated the reach and efficacy of machine learning, but has also emphasised long-standing issues that this technology has been unable to address. A principal challenge is represented by limited or biased datasets that can lead a learner to focus on spurious correlations in the training data that are harmful to deployment. Both, the investigation and systematic manipulation of a model’s distributed representations, are of significant importance to address related safety, fairness and performance concerns.

In this context, particular progress has been made in the qualitative analysis of factors of importance via visualisations of features which maximally activate individual or sets of units (see, for example, [Yosinski et al., 2015, Erhan et al., 2009, Simonyan et al., 2013, Selvaraju et al., 2016, Olah et al., 2017, 2018, Fong and Vedaldi, 2017, 2018]). While these methods are coarsely indicative of which parts of the input have a significant influence on the network’s output, these visualisations are often found to be insensitive to the nuances of intermediate representations [Mahendran and Vedaldi, 2016a]. For instance, Selvaraju et al. [2017] show that the visualisation of a network’s attention map over an input image does not change even for artificially crafted adversarial examples which maximally confuse the classifier.

We posit that, despite an clear established need, more consistent systematic and methodical frameworks are missing to investigate and manipulate model representations with respect to the kind of biases present and how these affect predictions. In particular, we desire the ability to query a model

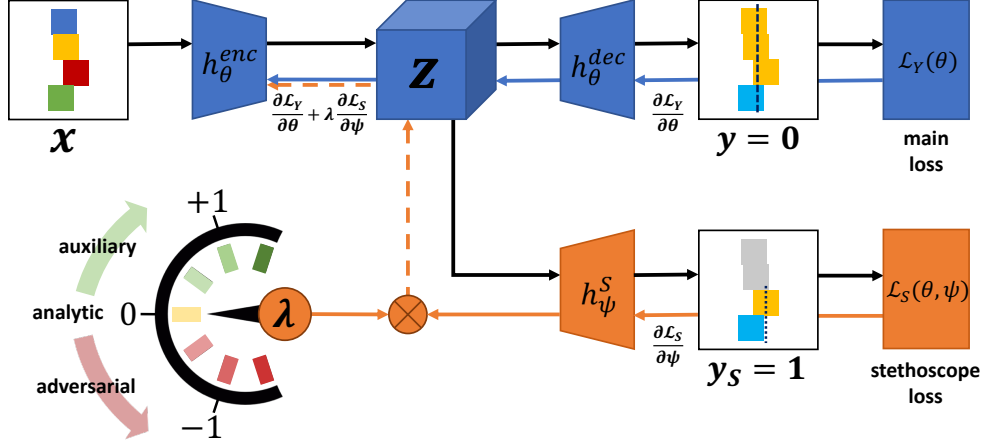


Figure 1: The stethoscope methodology presented with block tower stability prediction as an exemplary task. The main network (blue), comprised of an encoder and a decoder, is trained for global stability prediction. The stethoscope (orange), a two layered perceptron, is trained to predict a nuisance parameter (local stability) where the input is Z , a learned feature from an arbitrary layer of the main network. The stethoscope loss is back-propagated with weighting factor λ to the main network. The value of λ determines whether the stethoscope operates in analytic ($\lambda = 0$), auxiliary ($\lambda > 0$) or adversarial manner ($\lambda < 0$).

for *specific* biases via non-intrusive interrogation and to actively suppress or promote information in intermediate representations which improves the main task of the model.

Towards this goal we note that much of the required machinery already exists in a number of sub-domains of deep learning. Work on auxiliary objectives [Jaderberg et al., 2016] as well as multi-task learning (e.g. [Caruana, 1995, 1998]) commonly utilise dedicated modules with losses targeted towards a variety of tasks in order to optimise a representation shared across tasks. Based on this notion both *deep supervision* [Wang et al., 2015] and *linear classifier probes* [Alain and Bengio, 2016] were introduced as a way to reinforce the original loss signal at various levels throughout a network stack. Although their work is restricted to reinforcing the learning signal via the same loss applied to the global network, [Alain and Bengio, 2016], in particular demonstrate that the accessibility of information at a given layer can be determined - and promoted - by formulating a loss applied locally to that layer. Conversely, in order to encourage representations invariant to components of the input signal, regularisation techniques are commonly utilised (e.g. [Srivastava et al., 2014]). To more specifically obtain invariance with respect to known, systematic changes between training and deployment data, methods for domain adaptation [Ganin et al., 2016, Wulfmeier et al., 2017] and work on pivots in physics applications [Louppe et al., 2017] employ adversarial training frameworks to encode relevant properties such that they cannot be easily decoded by an adversary.

Inspired by this prior art and motivated by a need for effective tools to enhance interpretability and performance of deep models, in this work we present *neural stethoscopes* as a unified framework for the interrogation and perturbation of task-specific information at any layer. A stethoscope can be deployed in a purely *analytic* fashion whereby a fine-grained question is posed via a stethoscope loss which is not propagated back into the main network. It can also be used to promote or suppress specific information by deploying either an auxiliary or an adversarial training mechanism. The concept is illustrated in Figure 1. Specifically, we demonstrate that deploying an auxiliary stethoscope can be used to promote information conducive to the main task, thus improving overall network performance. Conversely, we demonstrate that an adversarial stethoscope can mitigate a specific bias by effectively suppressing information which hinders a network’s success. Moreover, the main network does not need to be changed in order to apply a neural stethoscope.

While neural stethoscopes find application in many domains, we choose here the emerging field of intuitive physics as a testing ground for our ideas. In particular, we focus on vision-based stability prediction for block towers which provides a convenient example of two well-defined and visually related, yet *provably* independent concepts: local and global stability. Using the publicly available

ShapeStacks dataset [Groth et al., 2018], we show that local object stability in block towers provides a strong visual signal exerting a disproportionate influence on global stability prediction despite being physically irrelevant. Furthermore, we show that suppressing this information via an adversarial stethoscope results in a significant performance increase, effectively de-biasing the model, while promoting it via an auxiliary stethoscope leads to further performance impairment by increasing the bias. In the same vein, we demonstrate that promoting other complementary information leads to additional gains.

2 Related Work

The notion of passively interrogating and actively influencing feature representations in hidden layers of neural networks connects disparate fields including interpretability, auxiliary losses and multitask learning as well as adversarial training.

Interpretability Recent successes in obtaining insights into distributed representations of neural models build on approaches for the generation or visualisation of features represented by single neurons [Yosinski et al., 2015, Erhan et al., 2009, Mahendran and Vedaldi, 2016b, Zeiler and Fergus, 2013], groups of neurons [Olah et al., 2018] or complete layers [Raghu et al., 2017] as well as the extraction of maximally exciting image patches from a dataset [Olah et al., 2017]. Saliency detection methods [Simonyan et al., 2013, Selvaraju et al., 2016, Dabkowski and Gal, 2017], compute heat-maps over the input representation to determine regions of high influence on the final network prediction.

On the quantitative side, different methods aim to provide insight into the learning dynamics and representations [Raghu et al., 2017, Bau et al., 2017]. The most relevant work to our analytic application of stethoscopes is given by Alain and Bengio [2016], who introduce linear classifier probes but limit their application, evaluation and discussion to the same objective for probes and the main network. Additional similarities exist to work of Mirowski et al. [2016], Jaderberg et al. [2016], who use small auxiliary networks to assess and manipulate reinforcement agents’ representations with respect to various supplemental tasks.

Auxiliary Objectives and Multitask Learning Auxiliary stethoscopes can be used to guide the learning of the main model by providing an additional learning signal. Reinforcement learning has been shown to benefit from such approaches, both in terms of sample efficiency and final performance [Mirowski et al., 2016, Jaderberg et al., 2016]. Multitask learning [Caruana, 1995, 1998] represents another use case where representations are optimised for multiple objectives, aiming to promote feature learning and to result in increased performance on all tasks. This is different from auxiliary training since, for the latter, the performance on the supplemental task is not important; the only purpose of it is to improve learning on the main task. Additional advantages lie in the context of optimisation challenges, such as vanishing gradients [Szegedy et al., 2015, Wang et al., 2015, Alain and Bengio, 2016]. Optimising auxiliary classifiers connected to early and intermediate layers of the main network provides a stronger learning signal and encourages learning of discriminative features in earlier layers.

Regularisation and Invariance Overfitting describes the problem of a model fitting to correlations between features and labels of the training data which do not generalise to external holdout data. Different forms of regularisation, such as L1/L2 regularisation or dropout Srivastava et al. [2014], aim to render a model invariant to such features by introducing general assumptions for the model.

In order to prevent a model to fit to a more specific nuisance factor Louizos et al. [2015] minimise the Maximum Mean Discrepancy (MMD) between conditional distributions with different values of a binary nuisance variable in the conditioning set. This method is limited to discrete nuisance variables and has a computational scaling exponentially in the number of states available. Xie et al. [2017] address both issues via adversarial training, optimising an encoding to confuse an additional discriminator, which aims to determine the nuisance parameters’ values. This approach assumes that the nuisance variable is known and is an input to the main model during training and deployment. Louppe et al. [2017] follow a similar approach, applying the discriminator to the output of the main model instead of its intermediate representations. However, due to similarities to generative adversarial networks [Goodfellow et al., 2014], adversarial applications can build on different formulations for its objective [Goodfellow et al., 2014, Arjovsky et al., 2017, Louppe et al., 2017].

In this work, we deploy concepts from interpretability and multitask learning to determine the accessibility of specific factors throughout the layers of a deep model and utilise auxiliary or adversarial training as appropriate to promote or suppress this information respectively.

3 Neural Stethoscopes

In supervised learning, we typically look for a function $f_\theta : X \rightarrow Y$ with parameters θ that maps an input $x \in X$ to its target $y \in Y$. Often the function internally computes one or more intermediate representations $z \in Z$ of the data. In this case, we rewrite f_θ as the composition of the encoder $h_\theta^{\text{enc}} : X \rightarrow Z$, which maps the input to the corresponding features $z \in Z$, and the decoder $h_\theta^{\text{dec}} : Z \rightarrow Y$, which maps features to the output.

In this work we consider only classification tasks, so that Y is a finite set of labels (or a simplex in the case of a probabilistic output), but our approach generalises directly to any regression task.

The information present in the input x might support a number of different tasks. We define a task $y : X \rightarrow Y$ to be an assignment $y = y(x)$ of the data points x to labels in some space Y . We further divide the space of tasks \mathcal{T} into \mathcal{Y} , the space of tasks we care about, and $\mathcal{S} = \mathcal{Y}^c$, all *supplemental* ones.

It is crucial that tasks $s \in \mathcal{S}$ might or might not be related to tasks $y \in \mathcal{Y}$. Specifically, we say that two tasks are unrelated if their corresponding target labels are uncorrelated and their feature representation required to solve the task are uncorrelated. While simultaneous learning of related tasks might improve performance on all of them [Caruana, 1998], it is often unclear which tasks are related. It is not enough to look at correlations, since one of the tasks in \mathcal{S} might be seemingly correlated with the target task y , *e.g.*, due to the limited size of the training data or bias present therein, when the tasks are actually unrelated or independent. In such scenarios, a mechanism that would allow to identify whether some tasks are related or not would be useful. Consequently, an ability to enforce independence or correlation between certain tasks, whether it is known or suspected, would be valuable.

To this end, we define the neural stethoscope framework, which unifies the above aspects and allows to (1) determine to what degree a task is supported by a given learnt representation, as well as (2) enforce correlation or independence between a representation and a task via auxiliary or adversarial training.

Let the stethoscope be defined as an arbitrary function $h_\psi^s : Z \rightarrow S$ with parameters ψ . Crucially, h_ψ^s is trained on a supplemental task with targets $s \in S$ and not for the main objective. We define two loss functions: $\mathcal{L}_y(\theta)$, which measures the discrepancy between predictions f_θ and the true task y and $\mathcal{L}_s(\theta, \psi)$, which measures the performance on the supplemental task.

The weights of the stethoscope are updated as $-\Delta\psi \propto \nabla_\psi \mathcal{L}_s(\theta, \psi)$ to minimise $\mathcal{L}_s(\theta, \psi)$ and the weights of the main network as $-\Delta\theta \propto \nabla_\theta \mathcal{L}_{y,s}(\theta, \psi)$ to minimise the energy

$$\mathcal{L}_{y,s}(\theta, \psi) = \mathcal{L}_y(\theta) + \lambda \cdot \mathcal{L}_s(\theta, \psi). \quad (1)$$

By choosing different values for the constant λ we obtain three very different use cases:

Analytic Stethoscope ($\lambda = 0$) Here, the gradients of the stethoscope, which acts as a passive observer, are not used to alter the main model. This setup can be used to interrogate learned feature representations: if the stethoscope predictions are accurate, the features can be used to solve the task.

Auxiliary Stethoscope ($\lambda > 0$) In this case, the encoder is trained with respect to the stethoscope objective, hence effectively enforcing correlation between representations used to solve both the main and supplemental tasks. This setup is related to learning with auxiliary tasks, and helpful if we expect the two tasks to be beneficially related.

Adversarial Stethoscope ($\lambda < 0$) By setting $\lambda < 0$, we can train the encoder to maximise the stethoscope’s loss (which the stethoscope *still* tries to minimise), thus encouraging independence between the main network and a supplemental tasks. This is effectively an adversarial training framework and is useful if features required to solve the stethoscope task are a detrimental nuisance factor.

For the analytic stethoscope, to fairly compare the accessibility of information with respect to a certain task in different feature representations, we set two criteria: (1) The capacity of the stethoscope

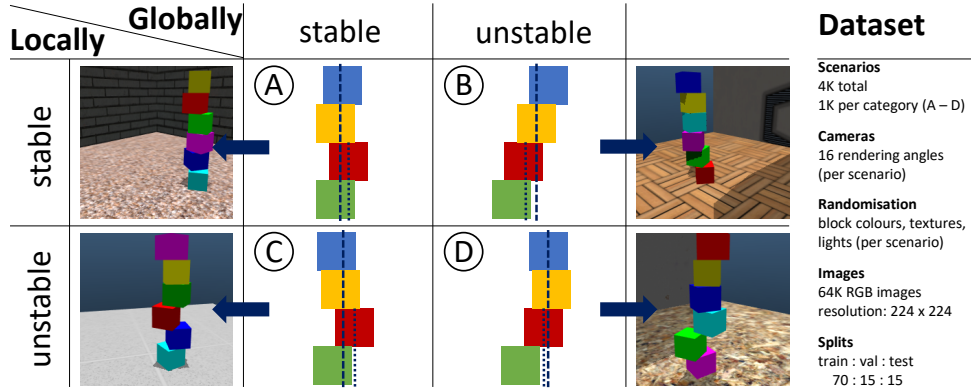


Figure 2: We have four qualitative scenarios: (A) Globally stable towers which also do not exhibit any local stability violation. (B) Towers without any local instability which are globally unstable because of the skew. (C) Towers in which one local stability violation is counterbalanced by blocks above. (D) Globally unstable towers where the site of local and global violation is perfectly correlated. The dashed line shows the projection of the cumulative centre of mass of the upper tower (red, yellow and blue block) whereas the dotted line depicts the projection of the local centre of mass of the red block. A tower is globally stable, if and only if the global centre of mass is always supported whereas the individual local centre of masses are not indicative of global structure stability. Global and local centre of masses for the green, yellow and blue block have been omitted for clarity of presentation.

architecture has to be constant regardless of the dimensions of its input. (2) The stethoscope has to be able to access each neuron of the input separately.

We guarantee this by fully connecting the input with the first layer of the stethoscope using a sparse matrix. This matrix has a constant number of non-zero entries (criterion 1) and connects every input unit to at least one unit of the first layer in the stethoscope (criterion 2). Furthermore, we guarantee that each unit in the first layer of the stethoscope is connected to at least one unit in the input and that, for either side, the number of connections per unit is uniformly distributed.

In auxiliary and adversarial mode, we attach the stethoscope to the main network’s last layer before the logits in a fully connected manner. During our experiments this setup proved to have the highest impact on the learning process of the main network. The stethoscope itself is implemented as a two-layer perceptron with ReLU activation and trained with sigmoid or softmax cross-entropy loss on its task \mathcal{S} .

For numerical stability, the loss of the encoder in the adversarial setting is rewritten as

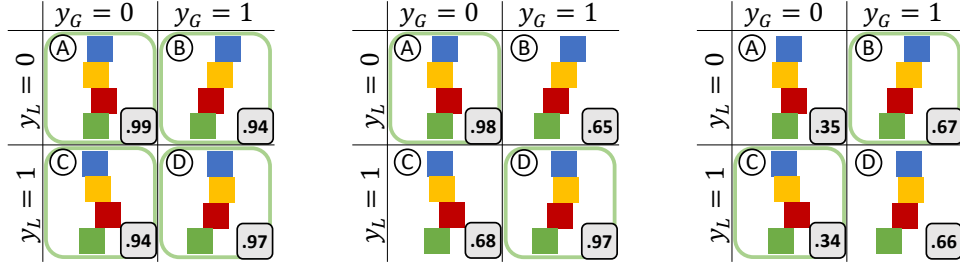
$$\tilde{\mathcal{L}}_{y,s}(\theta, \psi) = \mathcal{L}_y(\theta) + |\lambda| \cdot \mathcal{L}_{\bar{s}}(\theta, \psi) \quad (2)$$

where $\mathcal{L}_{\bar{s}}(\theta, \psi)$ is the stethoscope loss with flipped labels. The objective is similar to the confusion loss formulation utilised in GANs to avoid vanishing gradients when the discriminator’s performance is high [Goodfellow, 2016].

4 Vision-Based Stability Prediction of Block Towers

As our main test case for the methodology developed in Section 3 we choose neural networks for visual prediction of physical phenomena as described in this section.

Physics prediction with neural networks has received increasing attention in the community. A representative example is the task of predicting the stability of object stacks [Lerer et al., 2016, Wu et al., 2017, Groth et al., 2018], which is a well-suited test case for the proposed stethoscope framework for multiple reasons: firstly, scenarios have independent physical properties, namely the global/local stability of the stacks, that are however visually entangled; secondly, the analysis conducted by [Lerer et al., 2016, Groth et al., 2018] suggests that neural networks attend to correct image regions pertaining to structural stability but leave open whether this is due to sound physical



(a) Trained on All: $\varnothing_{acc} = 0.96$ (b) Trained on Easy: $\varnothing_{acc} = 0.82$ (c) Trained on Hard: $\varnothing_{acc} = 0.51$

Figure 3: The influence of local instability on global stability prediction. In setup (a) we train on all 4 tower categories (indicated by green frames). Global stability prediction accuracies on per-category test splits are reported in the bottom right grey boxes. In (b) we train solely on easy scenarios (A & D) where global and local stability are positively correlated. In (c) we only present hard scenarios during training featuring a negative correlation between global and local stability. The performance differences clearly show that local stability influences the network’s prediction for global stability.

reasoning or biases in the training data; and, lastly, the public availability of the *ShapeStacks* environment [Groth et al., 2018] facilitates experimentation in this setting.

Dataset As shown in Groth et al. [2018], a single-stranded tower of blocks is stable if, and only if, at every interface between two blocks the centre of mass of the entire tower above is supported by the convex hull of the contact area. If a tower satisfies this criterion, *i.e.*, it does not collapse, we call it *globally stable*. Moreover, we call it *locally stable* if, and only if, at every interface between two blocks, the centre of mass of the block immediately above is supported by the convex hull of the contact area. Intuitively, this measure describes if taken on its own, without any blocks above, each block would be stable. We associate binary prediction tasks y_G and y_L to resp. global and local stability where label $y = 0$ indicates *stability* and $y = 1$ *instability*. Global and local instability are neither mutually necessary nor sufficient, but can easily be confused visually which is demonstrated by our experimental results. Based on the two factors of local and global stability, we create a simulated dataset¹ with 4,000 block tower scenarios divided into four qualitative categories (cf. Figure 2). The dataset is divided into an *easy* subset, where local and global stability are always positively correlated, and a *hard* subset, where this correlation is always negative.

Model We chose the Inception-v4 network [Szegedy et al., 2017] as it yields state-of-the-art performance on stability prediction [Groth et al., 2018]. The model is trained in a supervised setting using example tuples (x, y_G, y_L) consisting of an image x and its global and local stability labels y_G and y_L . Classification losses use sigmoid cross entropy. We use the RMSProp optimiser [Tieleman and Hinton, 2012] throughout all our experiments.²

Local Stability as a Visual Clue Based on the four categories of scenarios described in Figure 2, we conduct an initial set of experiments to gauge the influence of local stability on the network predictions. If local stability had, as it would be physically correct, no influence on the network’s prediction of global stability, the performance of the network should be equal for *easy* and *hard* scenarios, regardless of the training split. However, Figure 3 shows a strong influence of local stability on the prediction performance. When trained on the entire, balanced data set, the error rate is three times higher for hard than for easy scenarios (6% vs. 2%). When trained on easy scenarios only, the error rate even differs by a factor of 13. Trained on hard scenarios only, the average performance across all four categories is on the level of random chance (51%), indicating that negatively correlated local and global stability imposes a much harder challenge on the network.

5 Using Neural Stethoscopes to Enhance Visual Stability Prediction

After demonstrating the influence of local stability on the task of global stability prediction we turn our attention to the use of neural stethoscopes to quantify and actively mitigate this influence.

¹We use the MuJoCo physics engine [Todorov et al., 2012] for rendering and stability checking.

²We use the Tensorflow [Abadi et al., 2016] implementation of RMSProp without momentum, gradient history decay of 0.9, epsilon of 1.0, a learning rate of 0.045 and a learning rate decay of 0.975 after every epoch.

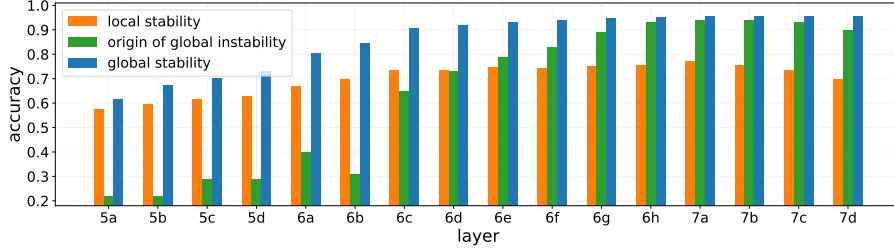


Figure 4: Analysis of the prediction performance throughout the Inception-v4 network trained on predicting global stability. We report average performances on balanced test data after 50 epochs of stethoscope training. All stethoscopes have been attached to the respective activation tensors³ with sparse connection matrices as described in Section 3.

Task Relationship Analysis We seek to quantify the correlation of features extracted for global stability prediction with the task of local instability detection. To this end, we train the main network on global stability prediction while attaching stethoscopes to multiple layers. For a holistic analysis, the stethoscope is trained on three tasks: global stability prediction (binary), local stability prediction (binary) and prediction of the origin of global instability, particularly the interface at which this occurs (n-way one-hot). Figure 4 reveals that the network gradually builds up features which are conducive to both global and local stability prediction. However, we observe that the performance of local stability prediction peaks at the activation tensor after layer 7a whereas the performance for global stability prediction (both binary and n-way) keeps improving. This is in line with the governing physical principles of the scenarios and yields the conjecture that the information about local stability can be considered a *nuisance factor* in this setup whereas information about the global site of stability violation can serve as a *complementary factor* for the main task.

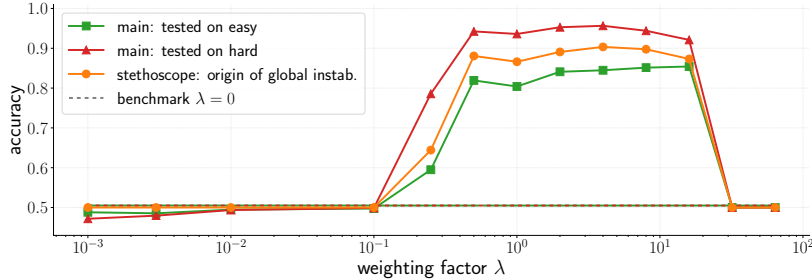


Figure 5: Performance gains by promoting complementary feature extraction with auxiliary stethoscopes. The main network is trained on binary global stability labels while the stethoscope is trained on more fine grained labels - origin of global stability (n-way). The network was trained on *hard* scenarios only but evaluated on all. The dashed lines represent baselines for $\lambda = 0$.

Promotion of Complementary Information We now test the hypothesis that fine-grained labels of instability locations strongly correlate with features of general global stability and that promoting this feature helps the main network to grasp the correct physical concepts. To that end, we consider the setup from Figure 3c where the training data only consists of *hard* scenarios with a baseline performance of 51%. The main network is trained on global stability while the stethoscope is trained on predicting the origin of global instability. Figure 5 shows that auxiliary training substantially improves the performance for weighting parameters $\lambda \in [0.5, 16]$. However, for very small values of λ , the contribution of the additional loss term is too small while for large values, performance deteriorates to the level of random chance, presumably due to very large gradients.

Suppression of Nuisance Information Results from Figure 3 indicate that the network might use local stability as a visual clue to make biased assumptions about global stability. We now investigate whether it is possible to debias the network by forcing it to pay less attention to local stability. To that end, we focus on the scenario shown in Figure 3b, where we only train the network on global stability

³The stethoscopes are connected to outputs of inception and reduction modules of the Inception v4 network, cf. Szegedy et al. [2017]. Note that this analysis is specific to this architecture and could yield very different results e.g. for networks with residual connections.

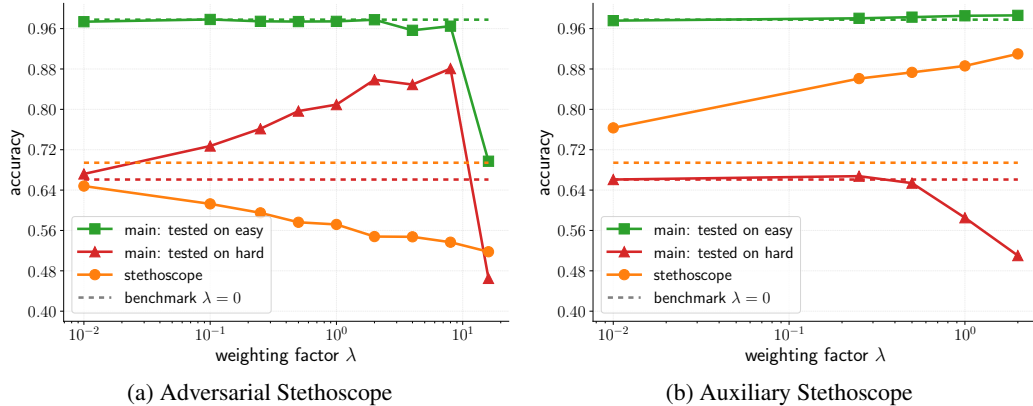


Figure 6: Successful debiasing by suppressing a nuisance factor with adversarial training while auxiliary training worsens the bias. The main network is trained on global stability while the supplementary task is to predict presence of local instabilities. Training data for global stability only comprises *easy* scenarios while training data for the supplementary task comprises both *easy* and *hard* scenarios. Green squares and red triangles show accuracies of the main network when predicting global stability of block towers for *easy* scenarios and *hard* scenarios, respectively. Orange circles depict the performance of the stethoscope on the task of local stability.

labels for *easy* scenarios. As shown in Figure 3b, the performance of the network suffers significantly when tested on *hard* scenarios where local and global stability labels are inversely correlated.

The hypothesis is that forcing the network not to focus on local stability weakens this bias. In Figure 6, we use active stethoscopes ($\lambda \neq 0$) to test this hypothesis. We train a stethoscope on local stability on labels of all categories (in a hypothetical scenario where local labels are easier to obtain than global labels) and use both the adversarial and the auxiliary setup in order to test the influence of suppressing and promoting accessibility of information relevant for local stability in the encoded representation, respectively. In Figure 6, the results of both adversarial and auxiliary training are compared to the baseline of $\lambda = 0$, which is equivalent to the analytic stethoscope setup.

Figure 6a shows that adversarial training does indeed partly remove the bias and significantly increases the performance of the main network on *hard* scenarios while maintaining its high accuracy on *easy* scenarios. The bias is removed more and more with increasing magnitude of the weighting factor λ up to a point where further increasing λ jeopardises the performance on the main task as the encoder puts more focus on confusing the stethoscope than on the main task (in our experiments this happens at $\lambda \approx 10^1$). Naturally, the performance of the stethoscope continuously decreases with increasing λ as the encoder puts more and more focus on confusing the stethoscope.

This scenario could also be seen from the perspective of feeding additional information into the network, which could profit from more diverse training data. However, Figure 6b shows that naively using an auxiliary setup to train the network on local stability worsens the bias. With increasing λ and increasing performance of the stethoscope, the network slightly improves its performance on *easy* scenarios while accuracy deteriorates on *hard* scenarios. These observations are readily explained: local and global stability are perfectly correlated in the *easy* scenarios, *i.e.*, the (global) training data. The network is essentially free to choose whether to select local or global features when predicting global stability. Auxiliary training on local stability further shifts the focus to local features. When tested on *hard* scenarios, where local and global stability are inversely correlated, the network will therefore perform worse when it has learned to rely on local features.

6 Discussion

We introduced the framework of *neural stethoscopes* unifying multiple threads of work in machine learning related to analytic, auxiliary and adversarial probing of neural networks. We selected the task of stability prediction of block towers as a proof-of-concept application due to the clear set of underlying physical rules and the explicit control over nuisance factors which confuse neural-network-based visual classifiers. The analytic application of stethoscopes allows to measure relationships between different prediction tasks and thus prove or disprove them. In addition to the analysis,

the auxiliary and adversarial modes of the stethoscopes can be used to support a main task by promoting beneficial complementary information and suppressing harmful nuisance information without changing the network architecture of the main predictor. This especially yields substantial performance gains in unfavourable training conditions where data is biased or labels are partially unavailable.

Acknowledgements

This research was funded by the EPSRC AIMS Centre for Doctoral Training at Oxford University and the European Research Council under grant ERC 677195-IDIU. We thank Adrian Penate-Sanchez, Oliver Bartlett and Triantafyllos Afouras for proofreading.

We acknowledge use of Hartree Centre resources in this work. The STFC Hartree Centre is a research collaboratory in association with IBM providing High Performance Computing platforms funded by the UK's investment in e-Infrastructure. The Centre aims to develop and demonstrate next generation software, optimised to take advantage of the move towards exa-scale computing.

References

- Martin Abadi, Paul Barham, Jianmin Chen, Zhifeng Chen, Andy Davis, Jeffrey Dean, Matthieu Devin, Sanjay Ghemawat, Geoffrey Irving, Michael Isard, Manjunath Kudlur, Josh Levenberg, Rajat Monga, Sherry Moore, Derek G. Murray, Benoit Steiner, Paul Tucker, Vijay Vasudevan, Pete Warden, Martin Wicke, Yuan Yu, and Xiaoqiang Zheng. Tensorflow: A system for large-scale machine learning. In *12th USENIX Symposium on Operating Systems Design and Implementation (OSDI 16)*, pages 265–283, 2016. URL <https://www.usenix.org/system/files/conference/osdi16/osdi16-abadi.pdf>.
- Guillaume Alain and Yoshua Bengio. Understanding intermediate layers using linear classifier probes. In *International Conference on Learning Representations (ICLR) Workshop*, 2016.
- Martin Arjovsky, Soumith Chintala, and Léon Bottou. Wasserstein gan. *arXiv*, 1705.10279, 2017. URL <https://arxiv.org/abs/1701.07875>.
- David Bau, Bolei Zhou, Aditya Khosla, Aude Oliva, and Antonio Torralba. Network dissection: Quantifying interpretability of deep visual representations. In *Computer Vision and Pattern Recognition (CVPR), 2017 IEEE Conference on*, pages 3319–3327. IEEE, 2017.
- Rich Caruana. Learning many related tasks at the same time with backpropagation. In *Advances in neural information processing systems*, pages 657–664, 1995.
- Rich Caruana. Multitask learning. In *Learning to learn*, pages 95–133. Springer, 1998.
- Piotr Dabkowski and Yarín Gal. Real time image saliency for black box classifiers. In *Advances in Neural Information Processing Systems*, pages 6970–6979, 2017.
- Dumitru Erhan, Yoshua Bengio, Aaron Courville, and Pascal Vincent. Visualizing higher-layer features of a deep network. *University of Montreal, Technical Report*, 1341(3):1, 2009.
- Ruth Fong and Andrea Vedaldi. Net2vec: Quantifying and explaining how concepts are encoded by filters in deep neural networks. In *The IEEE Conference on Computer Vision and Pattern Recognition (CVPR)*, July 2018.
- Ruth C Fong and Andrea Vedaldi. Interpretable explanations of black boxes by meaningful perturbation. In *The IEEE International Conference on Computer Vision (ICCV)*, Oct 2017.
- Yaroslav Ganin, Evgeniya Ustinova, Hana Ajakan, Pascal Germain, Hugo Larochelle, François Laviolette, Mario Marchand, and Victor Lempitsky. Domain-adversarial training of neural networks. *The Journal of Machine Learning Research*, 17(1):2096–2030, 2016.
- Ian Goodfellow. Tutorial: GANs. *arXiv*, 2016. ISSN 0253-0465. doi: 10.1001/jamainternmed.2016.8245.
- Ian Goodfellow, Jean Pouget-Abadie, Mehdi Mirza, Bing Xu, David Warde-Farley, Sherjil Ozair, Aaron Courville, and Yoshua Bengio. Generative adversarial nets. In *Advances in neural information processing systems*, pages 2672–2680, 2014.
- Oliver Groth, Fabian Fuchs, Ingmar Posner, and Andrea Vedaldi. Shapestacks: Learning vision-based physical intuition for generalised object stacking. *arXiv*, 1804.08018, 2018.
- Max Jaderberg, Volodymyr Mnih, Wojciech Czarnecki, Tom Schaul, Joel Z. Leibo, David Silver, and Koray Kavukcuoglu. Reinforcement learning with unsupervised auxiliary tasks. *CoRR*, abs/1611.05397, 2016.
- Adam Lerer, Sam Gross, and Rob Fergus. Learning physical intuition of block towers by example. In *Proceedings of the 33rd International Conference on International Conference on Machine Learning - Volume 48, ICML 16*, pages 430–438. JMLR.org, 2016. URL <http://dl.acm.org/citation.cfm?id=3045390.3045437>.
- Christos Louizos, Kevin Swersky, Yujia Li, Max Welling, and Richard S. Zemel. The variational fair autoencoder. *CoRR*, abs/1511.00830, 2015.
- Gilles Louppe, Michael Kagan, and Kyle Cranmer. Learning to pivot with adversarial networks. In *NIPS*, 2017.
- Aravindh Mahendran and Andrea Vedaldi. Visualizing deep convolutional neural networks using natural pre-images. *International Journal of Computer Vision*, 120(3):233–255, Dec 2016a. ISSN 1573-1405. doi: 10.1007/s11263-016-0911-8. URL <https://doi.org/10.1007/s11263-016-0911-8>.
- Aravindh Mahendran and Andrea Vedaldi. Visualizing deep convolutional neural networks using natural pre-images. *International Journal of Computer Vision*, 120(3):233–255, 2016b.

- Lars Mescheder, Sebastian Nowozin, and Andreas Geiger. The numerics of gans. In I. Guyon, U. V. Luxburg, S. Bengio, H. Wallach, R. Fergus, S. Vishwanathan, and R. Garnett, editors, *Advances in Neural Information Processing Systems 30*, pages 1825–1835. Curran Associates, Inc., 2017. URL <http://papers.nips.cc/paper/6779-the-numeric-of-gans.pdf>.
- Piotr W. Mirowski, Razvan Pascanu, Fabio Viola, Hubert Soyer, Andrew J. Ballard, Andrea Banino, Misha Denil, Ross Goroshin, Laurent Sifre, Koray Kavukcuoglu, Dharshan Kumaran, and Raia Hadsell. Learning to navigate in complex environments. *CoRR*, abs/1611.03673, 2016.
- Chris Olah, Alexander Mordvintsev, and Ludwig Schubert. Feature visualization. *Distill*, 2017. doi: 10.23915/distill.00007. <https://distill.pub/2017/feature-visualization>.
- Chris Olah, Arvind Satyanarayan, Ian Johnson, Shan Carter, Ludwig Schubert, Katherine Ye, and Alexander Mordvintsev. The building blocks of interpretability. *Distill*, 2018. doi: 10.23915/distill.00010. <https://distill.pub/2018/building-blocks>.
- Maithra Raghu, Justin Gilmer, Jason Yosinski, and Jascha Sohl-Dickstein. Svcca: Singular vector canonical correlation analysis for deep understanding and improvement. *arXiv preprint arXiv:1706.05806*, 2017.
- R. R. Selvaraju, M. Cogswell, A. Das, R. Vedantam, D. Parikh, and D. Batra. Grad-cam: Visual explanations from deep networks via gradient-based localization. In *2017 IEEE International Conference on Computer Vision (ICCV)*, pages 618–626, Oct 2017. doi: 10.1109/ICCV.2017.74.
- Ramprasaath R. Selvaraju, Abhishek Das, Ramakrishna Vedantam, Michael Cogswell, Devi Parikh, and Dhruv Batra. Grad-cam: Why did you say that? *CoRR*, abs/1611.07450, 2016.
- Karen Simonyan, Andrea Vedaldi, and Andrew Zisserman. Deep inside convolutional networks: Visualising image classification models and saliency maps. *arXiv preprint arXiv:1312.6034*, 2013.
- Nitish Srivastava, Geoffrey E. Hinton, Alex Krizhevsky, Ilya Sutskever, and Ruslan Salakhutdinov. Dropout: a simple way to prevent neural networks from overfitting. *Journal of Machine Learning Research*, 15: 1929–1958, 2014.
- Christian Szegedy, Wei Liu, Yangqing Jia, Pierre Sermanet, Scott Reed, Dragomir Anguelov, Dumitru Erhan, Vincent Vanhoucke, and Andrew Rabinovich. Going deeper with convolutions. In *Computer Vision and Pattern Recognition (CVPR)*, 2015. URL <http://arxiv.org/abs/1409.4842>.
- Christian Szegedy, Sergey Ioffe, Vincent Vanhoucke, and Alexander A Alemi. Inception-v4, inception-resnet and the impact of residual connections on learning. In *AAAI*, volume 4, page 12, 2017.
- T. Tieleman and G. Hinton. Lecture 6.5—RmsProp: Divide the gradient by a running average of its recent magnitude. COURSE: Neural Networks for Machine Learning, 2012.
- Emanuel Todorov, Tom Erez, and Yuval Tassa. MuJoCo: A physics engine for model-based control. *IEEE International Conference on Intelligent Robots and Systems*, pages 5026–5033, 2012. ISSN 21530858. doi: 10.1109/IROS.2012.6386109.
- Liwei Wang, Chen-Yu Lee, Zhuowen Tu, and Svetlana Lazebnik. Training deeper convolutional networks with deep supervision. *CoRR*, abs/1505.02496, 2015. URL <http://arxiv.org/abs/1505.02496>.
- Jiajun Wu, Erika Lu, Pushmeet Kohli, Bill Freeman, and Josh Tenenbaum. Learning to see physics via visual de-animation. In I. Guyon, U. V. Luxburg, S. Bengio, H. Wallach, R. Fergus, S. Vishwanathan, and R. Garnett, editors, *Advances in Neural Information Processing Systems 30*, pages 153–164. Curran Associates, Inc., 2017. URL <http://papers.nips.cc/paper/6620-learning-to-see-physics-via-visual-de-animation.pdf>.
- Markus Wulfmeier, Alex Bewley, and Ingmar Posner. Addressing appearance change in outdoor robotics with adversarial domain adaptation. In *IEEE/RSJ International Conference on Intelligent Robots and Systems*, October 2017.
- Qizhe Xie, Zihang Dai, Yulun Du, Eduard H. Hovy, and Graham Neubig. Controllable invariance through adversarial feature learning. In *NIPS*, 2017.
- Jason Yosinski, Jeff Clune, Thomas Fuchs, and Hod Lipson. Understanding neural networks through deep visualization. In *ICML Workshop on Deep Learning*. Citeseer, 2015.
- Matthew D. Zeiler and Rob Fergus. Visualizing and understanding convolutional networks. *CoRR*, abs/1311.2901, 2013. URL <http://arxiv.org/abs/1311.2901>.

A Appendix: Is Information Discarded in Adversarial Training?

Figure 6a shows that adversarial training increases performance given a biased training dataset. While hypothetically the network could learn to completely discard information about local stability when trying to confuse the adversarial stethoscope, it could also simply reduce its accessibility.

In an additional experiment (Figure 7), where the main network (blue line) is fixed after adversarial training for 120 epochs (grey dashed line), the performance of the stethoscope on local stability (orange) is fully recovered to the level of the baseline for a purely analytic stethoscope (dashed orange line). We therefore argue that the information is not removed, but instead made less accessible to the stethoscope by constantly shifting the representation as explained in [Mescheder et al., 2017]. However, the resulting performance increase for the main task indicates that this behaviour also makes information related to local stability less accessible to the decoder of the main network. Hence, although the adversarial setup does not reach final, stable equilibria (*cf.* [Mescheder et al., 2017]), it decreases the dependence of the decoder on features particular to local stability. Hence, further improvements for stabilising GAN training could additionally improve performance in adversarial stethoscope use-cases [Mescheder et al., 2017, Goodfellow, 2016, Arjovsky et al., 2017].

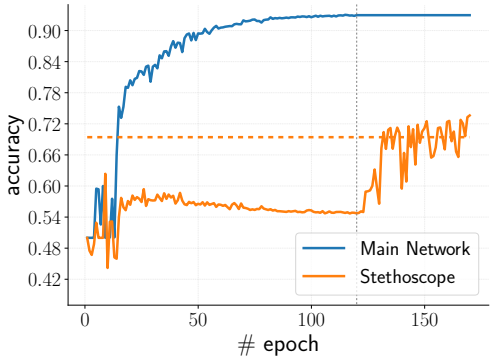


Figure 7: Stethoscope recovery after freezing the adversarially trained main network.

B Appendix: Suppressing Nuisance Information in MNIST

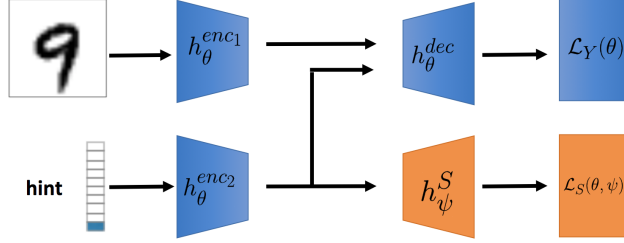
This section introduces two intuitive examples and serves to illustrate the challenge with biased training datasets. We conduct two toy experiments built on the MNIST dataset to demonstrate the issue of varying correlation between nuisance parameters and ground truth labels in training and test datasets and to demonstrate the use of an adversarial stethoscope to suppress this information and mitigate overfitting. Both experiments build on the provision of additional *hints* as network input. In the first experiment, the hint is a separately handled input in the form of a one-hot vector whereas in the second experiment, the hint is directly incorporated in the pixel space of the MNIST images.

In both experiments, the network is trained on the loss as defined in Equation (1) and the gradients are used to update the weights of the different parts of the network (encoder(s), decoder, stethoscope) as defined in Section 3. Hence, $\lambda < 0$ denotes adversarial training and $\lambda > 0$ auxiliary training.

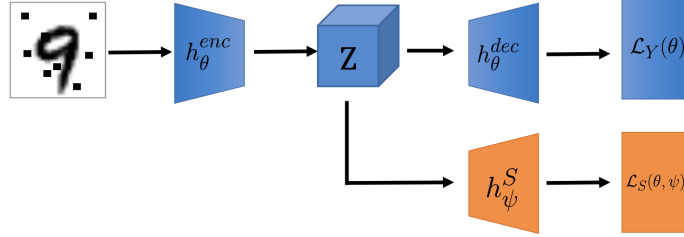
Hint as Separate One-Hot Vector In the first example, the hint labels have the same format as the true labels of the input image and we run experiments with varying correlation between hint and true label in the training set. Given high correlation, the network can learn an identity transformation between hint and output and ignore the image. Now, at test time, the hint is completely independent of the true label and hence contains no useful information. The experiment mimics challenges with biased datasets as the supplemental task $s \in \mathcal{S}$ (see Section 3) has labels \mathbf{y}_s which are correlated to the labels \mathbf{y} of the main objective during training but not at test time ($p_{train}(\mathbf{y}_s|\mathbf{y}) \neq p_{test}(\mathbf{y}_s|\mathbf{y})$). Hence, an approximation of the correlations in the training data will not generalise to data during deployment.

To that end, we introduce a parameter q_h denoting the quality of the hints (i.e. their correlation with the true labels) during training time where for $q_h = 1.0$, the hints are always correct (during training), for $q_h = 0.5$, the hints are correct for 50% of the training examples and so on. Varying the hint quality enables us to investigate biases of increasing strength.

In this setup (Figure 8a), both input streams are separated via independent encoders. Let $h_\theta^{enc_1}$ and $h_\theta^{enc_2}$ respectively denote image and hint encoders. The stethoscope only accesses the hint encoding in this example, which simplifies its task and enables us to demonstrate the effect of active stethoscopes without affecting the image encoding. The hint encoder multiplies the one-hot hint vector with a scalar weight. Hence, a weight close to zero would effectively hide the hint information



(a) First Toy Example: Hint as Separate One-Hot Vector



(b) Second Toy Example: Hint as Pixel Encoding

Figure 8: Setup of the toy experiments using the MNIST dataset with artificial hints. In (a), the hints are fed to the main network via a separate input and both input streams are encoded separately by neural networks. The stethoscope only sees the output of the hint encoder h_{θ}^{enc2} while the decoder h_{θ}^{dec} , which is trained on digit classification, sees the output of both encoders. In (b), the hints are incorporated as pixel modifications into the main images. The encoder h_{θ}^{enc} transforms the input into a latent representation Z which is then accessed by both the stethoscope h_{ψ}^S and the decoder h_{θ}^{dec} .

from the main network, explicitly making the task of the stethoscope h_{ψ}^S more difficult. The image encoder consists of two convolutional layers followed by two fully connected layers with 256 units where each layer is followed by leaky ReLU activations. The decoder h_{θ}^{dec} , which acts as a digit classifier, is comprised of a single fully connected layer and receives the image encoding concatenated with the encoded hint vector as input.

With adversarial training of the stethoscope, the encoder learns to suppress information about the hints forcing the classifier to purely rely on image data. As can be observed in Figure 9b, for perfect hints ($q_h = 1.0$) and no adversarial training, the decoder is highly accurate in predicting the hint (instead of the actual label), suggesting that the classifier is effectively independent of the input image and purely relies on the hint. With adversarial training, however, we can indeed force the encoder to hide the hint, therefore forcing it to learn to classify digits from images. As expected, with increasing hint quality, we need to increase the weight of adversarial training so as to discourage the encoder from relying on the hint.

Hint as Pixel Encoding In the second variant of the MNIST experiment, hints are provided at training time as a set of high intensity pixels in the input images as opposed to the explicit concatenation in the previous example. This better reflects the typical scenario where the goal is to disentangle the nuisance hints from the informative information related to the main task. Here, the main network is a two-layer multi-layer perceptron (MLP) with the stethoscope attached after the first hidden layer. The simpler architecture (compared to the one used in the first toy problem) was chosen in order to lower the performance on vanilla MNIST classification in order to see clearer effects. Note that in this setup, giving the same labels to the hints as for the main task in the training scenario makes the two tasks indistinguishable (in particular for perfect hint quality $h_q = 1.0$). We therefore introduce a higher number of hint classes with 100 different hints, each of them related to a single digit in a many-to-one mapping, such that theoretical suppression of hint information is possible without degrading main performance.

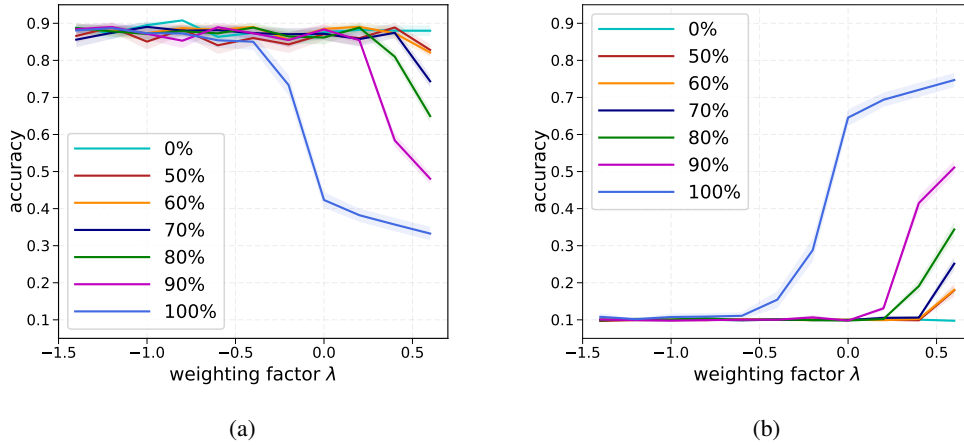


Figure 9: Influence of adversarial training on classifier performance for toy experiment variant 1 described in Figure 8a. Each curve represents the results for different hint qualities h_q . The bold lines indicate the mean of 100 runs and the shaded areas mark the student-t 1σ confidence intervals. In (a) the network is evaluated against the ground truth. In (b), the output of the network is compared to the hint labels during test time. Hence, a high accuracy in (b) shows strong overfitting while a high accuracy in (a) shows that the network learned the actual task of classifying digits from images.

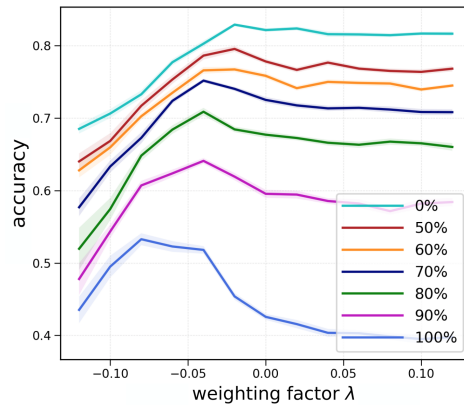


Figure 10: Influence of adversarial training on classifier performance for the second MNIST experiment. The adversarial training is less effective as both the stethoscope and the main network directly access a single encoding. High adversarial weights can strongly degrade performance on the main task as a trivial solution would be to suppress all information about the input. Each curve represents the results for different hint qualities h_q . The bold lines indicate the mean of 20 runs and the shaded areas mark the student-t 1σ confidence intervals.

Figure 10 shows the digit classification accuracy for the main network where the stethoscope is applied with weights ranging in both the positive and negative directions to reflect auxiliary and adversarial use of the stethoscope respectively. When using a positive stethoscope loss, which encourages h_{θ}^{enc} to focus more on the artificial hints over the actual digit features, the test accuracy degrades. This is expected for this toy example as the hints have zero correlation with the digit labels at test time. In the negative case, h_{θ}^{enc} serves as an adversary to the stethoscope effectively benefiting the main objectives by removing the misleading hint information leading to an improved test accuracy. However, as the magnitude of the adversarial strength increases the gains quickly erode as the encoder begins to suppress information relevant for the main task.